Coupled Hydro-Mechanical Behavior of Compacted Expansive Soil Based Material: Experimental and Numerical Investigations

Abhishek Rawat[a,*], Lin Zhi Lang[a], Anne-Catherine Dieudonne[b], Wiebke Baille[a], Frederic Collin[c]

[a] *Ruhr-Universität Bochum, Chair of Foundation Engineering, Soil and Rock Mechanics, Universitätsstr. 150, 44780 Bochum, Germany*
[b] *Faculty of Civil Engineering and Geosciences, Technical University Delft, Building 23, Stevinweg 1 2628 CN Delft, The Netherland*
[c] *Architecture, Geologie, Environnement and Constructions University of Liege, Quartier Polytech 1, Allee de la decouverte 9 - Batiment B52 4000 LIEGE, Belgium*

Abstract

This paper discusses the methodology for determining the parameters for use in the fully coupled hydro-mechanical analysis of the compacted bentonite based materials. The suction-controlled oedometer tests were performed to identify the Barcelona basic model parameters for the Calcigel bentonite sand mixture (50:50). It was observed that the collapse potential decreased with increasing the net stress, the observed behavior was contrary to the original Barcelona basic model. The model parameters were identified in a specific order and calibrated against the suction-controlled oedometer test results. In next-step, a fully coupled hydro-mechanical analysis was performed to simulate the laboratory-based water infiltration test using finite element method. The laboratory test was performed with an innovative column-type experimental device, which facilitated the simultaneous measurements of relative humidity, water content and stresses in both lateral and axial direction at various preselected locations along the height of soil sample. In the numerical analysis, the Barcelona basic model was used along with the dual porosity based soil water retention model for the compacted bentonite-based materials. The model results were in good agree-

*Corresponding author
Email address: abhishek.rawat@rub.de (Abhishek Rawat)

ment with the experimental measurements for the relative humidity and water content evolution over elapsed time. The predicted values of axial total stress at the hydration end also showed good agreement with the experimental measurements. However, some discrepancies were observed in the predicted and measured values of the lateral total stresses.
Keywords: Sealing material, Backfill material, LAGAMINE, Hydro mechanical behavior, Barcelona Basic Model.

1. Introduction

In Germany, the compacted bentonite-sand mixture (50:50) is proposed to use as a backfill material at the deep geological repository for the disposal of high and intermediate-level radioactive waste [1, 2, 3]. The primary function of backfill material is to create a low permeable zone for delaying the contact of ground water with the waste canister. The candidate backfill material possesses desirable characteristics such as low permeability, high sorption capability and adequate swelling potential, which allows it to fill the cracks and the constructional gaps at interfaces. The effectiveness of hydraulic barrier function of backfill material relies upon the ability of sealing the constructional gaps and cracks, which may act as preferential flow paths. In this regard, several field and laboratory based experimental investigations have been performed during the last few decades to better understand the hydro-mechanical coupling in the bentonite-based materials [4, 5, 6, 7, 8, 9, 10]. In general, the hydraulic and mechanical processes that take place within the backfill material during it's design period are strongly coupled and crucial from the design point of view. For instance, the rate of saturation and the resulting swelling pressure of the backfill material are inter-dependent. The mathematical formulations to reproduce this coupling is the key issue in the constitutive modeling for predicting the long-term behavior of backfill material under repository relevant boundary conditions.

Among the existing elasto-plastic constitutive models, the Barcelona basic

model proposed by Alonso et al. [11] is one of the first elastoplastic models for describing the mechanical behavior of the unsaturated soils. The model is the extension of the Modified Cam-Clay Model (MCCM) [12] for the unsaturated state by considering soil suction ($s = u_a - u_w$) as an additional stress variable. Several modifications have been suggested in the original formulations of the BBM [13, 14, 15, 16] to reproduce the swelling potential of the compacted bentonite-based materials. One of the major challenge in the application of BBM is the selection of material parameters, as the determination of parameters values from the experimental data is not straightforward. However, a few authors have suggested the guidelines for selecting the BBM parameters from the experimental investigations [17, 18, 19, 20].

Regarding the modeling of coupled flow and deformation problems, the indirect coupling is introduced by incorporating the soil water retention model, which features the description of soil suction and degree of saturation relationship in the mechanical constitutive model. The classical soil water retention models [21, 22, 23] are capable to capture the dependency of degree of saturation on soil suction for non-deformable soils in which the pore size distribution remains constant during wetting or drying path. For the deformable soils, several models have been proposed [24, 25, 26, 27, 28]. The above-mentioned models correlate the air entry/air expulsion suction with the void ratio or dry density of soil. Additionally, the double-structure water retention models have been proposed particularly for the compacted bentonite-based materials [32, 33, 34] based on the microstructural characteristics of bentonite in the compacted state. Clays in compacted form have multi-scale porosity domains [29, 30, 31]. Depending upon the mineralogy and the associated force fields, clay-water interaction mechanisms differ in these porosity domains. Based on these characteristics features, Dieudonne et al. [34] proposed a phenomenological model, which considers different water retention mechanisms in each structural levels of the compacted bentonite-based materials.

The present paper focuses on two main issues, the first one is related with the determination of model parameters of a fully coupled hydro-mechanical analy-

sis and the second one is related with the evaluation of predicting capabilities of the BBM along with the recently developed double structure water retention model [34] to capture the coupled hydro-mechanical behavior of compacted Calcigel bentonite-sand mixture (50:50). In this regard, a water infiltration test was conducted with an innovative column-type experimental device, which facilitated the simultaneous measurements of water content, relative humidity and the total stresses in both lateral and axial directions at various preselected locations. The resaturation of compacted soil sample was induced by supplying the distilled water from the bottom-end under the lateral and axial confinement. A fully coupled hydro-mechanical analysis of the test was performed with the finite element code LAGAMINE using the BBM and the double-structure water retention model proposed by Dieudonne et al. [34]. Prior to simulate the experiment, the characterization tests to determine the basic hydro-mechanical properties of the bentonite-sand mixture (50:50) were performed. These include the suction-controlled oedometer tests and water retention tests. The comparison between the predicted and measured values helped to identify the influencing factors which govern the coupled hydro-mechanical behavior of the investigated material.

2. Material

The investigated material was the compacted mixture of Calcigel bentonite and sand with equal dry mass ratio (50:50). Calcigel is a commercially available bentonite from the southern part of Germany with 60-70 % montmorillonite. It has a liquid limit of 180 %, plastic limit of 43-45 % and specific gravity of 2.80. The cation exchange capacity (CEC) is 74 meq/100 gm with 67 % of Ca^{+2} as a predominant exchangeable cation. Table 1 summarizes the relevant geotechnical properties of the tested materials. The Calcigel powder has 6 % hygroscopic moisture content. Prior to prepare a mixture with the oven-dried medium sand [35], the required volume of water was added to sand to achieve the mixture water content equal to 9 %. This method of preparing the

Table 1: Geotechnical properties of soil tested

Properties	Value
Bentonite	
Specific gravity	2.8
Liquid limit (%)	180
Plastic limit (%)	43-45
Shrinkage limit (%)	18-21
Plasticity index (%)	135-137
Sand	
Specific gravity	2.65
D10	0.25
D30	0.40
D60	0.70
Bentonite-sand mixture (50:50)	
Specific gravity	2.725
Liquid limit (%)	60
Plastic limit (%)	32
Plasticity index (%)	28

moist mixture gives less lump formations in the bentonite. Later, the moist-mixture was stored in a sealed plastic bag and kept in an airtight container for homogeneous moisture distribution for a period of 28 days.

3. Methods

3.1. Physical modeling: Column-type test device

Figure 1 shows the details of the newly designed column-type test device. The device is comprised of top and bottom plugs (items 1 and 5 in Figure 1a), sample rings (items S1, S2, and S3 in Figure 1a), and a confining cell (item 8). A rigid frame (item 9) provides the restraint along the axial direction. The stresses in the axial direction are measured using the load cells (items 6 and 7). The test set-up allows testing a cylindrical soil samples (dia. = 150 mm and height = 300 mm) and provides three measurement sections located at various heights from the bottom of the sample, such as X1 (50 mm), X2 (150 mm), and X3 (250 mm) (Figure 1a).

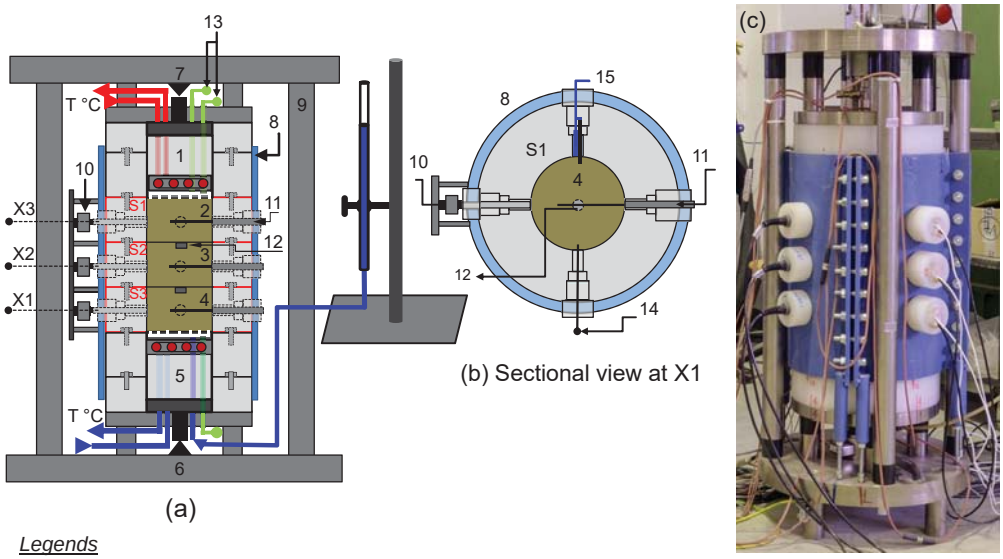

Figure 1: Constructional details of the newly designed column-type experimental set-up, (a) and (b) vertical and horizontal sectional views, and (c) a photograph of the device.

The top and bottom plugs have similar constructional features for applying the thermal and hydraulic gradients along the height of soil sample. The plug contains porous stainless-steel base (dia. = 150 mm and thickness = 10 mm), and a metallic chamber (dia. = 150 mm and thickness = 20 mm). The porous base has a water inlet and an air outlet that can be used in case of thermo-hydraulic tests. The metallic chamber accommodates the heating/cooling coil, which in turn is connected to an external thermostat (not shown). The heating/cooling temperature is controlled by circulating silicon oil in the coil with the precision of 0.1 °C. The integrated design of the metallic chamber with a porous base provides an adequate thermal equilibrium between the heating and hydration systems. These plugs transfer the axial total stress to the top and bottom load cells through a PVDF cylindrical piston (dia. = 148 mm and height = 100 mm). Polyvinylidene fluoride (PVDF) material provides suitable

thermal insulation for the heating unit.

To accommodate soil sample, three PVDF encapsulation rings/sample rings (outer dia. = 350 mm, inner dia. = 150 mm, and height = 100 mm) are used (i.e., S1, S2, and S3) (Figure 1). The PVDF sample rings assembly provide the mechanical stability, an adequate thermal insulation in the lateral direction, and accommodates the ports for the components of the monitoring sensors. Compacted soil samples can be prepared by compacting soil-water mixtures within each sample ring and further placed within the device. Each sample ring has four holes at the mid height, but radially positioned at an angle of 90° for installing the sensors that facilitate measuring temperature, relative humidity, water content, and lateral total stress (Figure 1b). The sensors are installed with their respective PVDF adaptors (Figure 1c) for minimizing the heat loss and any possible disturbances to the electronics of the sensors. The provision of O-ring connections along with tightening screws that are made of PVDF provide the air/water tight joints between two consecutive sample rings (Figure 1a). A stainless-steel confining cell is used to provide additional resistance against the outward lateral deformation of the sample rings during a test (Figure 1a). Additionally, the confining cell facilitates the installation of the lateral load cells (Figure 2a). A vertical stain-less steel plate provides a restraint for the lateral load cells (Figure 2b). The stiffness of the measuring system can be expected to be greater in the lateral direction than that in the axial direction due to the presence of constructional gaps and technical voids in the axial direction, which in turn may influence the development of total stress during the test.

3.2. Sample preparation and test method

The initial dry density of 1.80-1.85 Mg/m^3 with 6 to 9 % initial water content was suggested for the compacted bentonite-sand bricks as a backfill material according to the German reference concept for the disposal of low or intermediate level waste (LILWs) and high level waste (HLWs) [1, 2, 3]. In this regards, the mixture of Calcigel bentonite-sand with 9 % initial water content was compacted in three layers using uniaxial static compaction under 30 MPa in the vertical

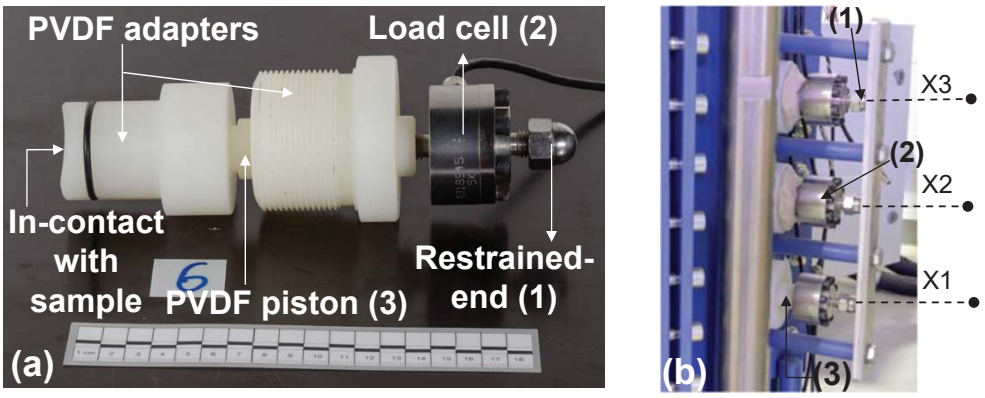

Figure 2: Lateral load cell installation details, (a) load cell along with accessories and (b) installation at measurement sections X1, X2 and X3 along the height of soil sample.

direction. During the compaction process, the surface of the compacted layer was scarified prior to place the next layer to ensure a proper homogeneous connection. The initial suction was measured using the chilled mirror hygroscope (26.9 MPa). After the compaction, the compacted block was extruded from the mould, the achieved mean dry density was 1.85 Mg/m^3 (block dia. = 153 mm; height = 100 mm). Total three blocks were compacted to achieve the required overall sample height of 300 mm.

It should be noted here that the compacted sample exhibited post-compaction strains during the extrusion process. Consequently, the sample diameter was slightly larger than the inner diameter of sample rings (i.e., 150 mm). Hence, these blocks were prepared for installing inside the sample ring with monitoring sensors after the extrusion from the mould. For installing the TDR wave-guides in to the compacted block, two parallel holes were drilled (dia. = 3.5 mm; length = 110 mm). Additionally, two holes were also drilled for inserting the Pt100 sensor (dia. = 6 mm; length = 10 mm) associated with VAISALA relative humidity sensor and an independent Pt100 sensor (dia. = 3 mm; length = 10 mm). For the installation of KYOWA miniature pressure transducers, a seating space was created during the compaction process using stainless steel dummy having dimensions identical to KYOWA pressure transducer. Figure 3 shows the compacted block with seating space for the installation of the KYOWA pressure

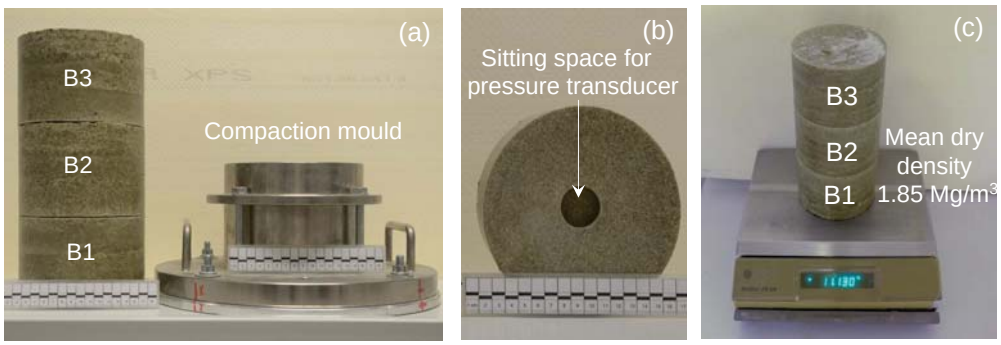

Figure 3: Sample preparation using static uniaxial compaction, (a) compacted blocks and compacting mould, (b) seating space for KYOWA pressure transducer and (c) average mean density.

transducer. The volume fractions of the sensors in the sample was only 0.14 % of the total sample volume (six Pt100 sensors, three TDR probes and two miniature pressure transducers). The TDR sensor constitutes of two parallel waveguides made of stainless steel and are coated with polyvinyl chloride for waterproofing. For correct measurements of the water content, the entire length of the probes must be embedded in the soil sample. These wave-guides are sensitive to deformation. Hence, the sensors embedment has insignificant effect on the sample response during the hydration under the confined conditions.

The test was conducted under the constant volume condition at room temperature; the air outlet at the bottom plug was kept closed, while the air outlet at top plug was kept open to evacuate the air during the hydration process. The site-specific ground water was replaced with the distilled water and supplied from the bottom-end under 15 kPa hydration pressure to mimic the water ingress from the host rock. Sensors along with data logger continuously monitored temperature, relative humidity, water content and total stress in both axial and lateral directions. The test was conducted for a period of 349 days. For the post-experimental measurements, the soil samples were collected from different locations along the height during the dismantling of test set-up. The relative humidity was measured using the Chilled Mirror technique, whereas the water content was measured using the standard oven-drying method.

3.3. Numerical modeling

A fully coupled hydro-mechanical analysis of the problem was performed using the finite element code LAGAMINE [36]. The Barcelona Basic Model (BBM) [11] and the water retention model proposed by Dieudonne et al. [34] were used to describe the elasto-plastic behavior of unsaturated expansive soils. The BBM [11] is a well-known elasto-plastic model, it is the extension of the Modified Cam-Clay Model [12] for the unsaturated state by considering soil suction as an additional stress variable.

Based on the experimental observations at both micro-and macroscales, Dieudonne et al. [34] proposed a phenomenological water retention model for the compacted bentonite. The model is developed to consider different water retention mechanisms in each structural level, namely adsorption in the intra-aggregate pore space (micro-scale) and capillarity in the inter-aggregate pore space (macro-scale). The consideration of different water retention mechanisms inside and between the aggregates allows for capturing the density effect on the soil water retention behavior. The model is formulated in terms of water ratio (e_w), which is expressed as the sum of a water stored in the micropores (e_{wm}) and the water contained in the macropores (e_{wM}). The water stored in the intra-aggregate pore space is based on the Dubinin's adsorption theory [37] as per Eq. 1,

$$\Omega_{wm} = \Omega_m exp\left\{-\left[\frac{RT}{\beta_D E_0} ln\left(\frac{\rho_v^0}{\rho_v}\right)\right]^{n_{ads}}\right\} \tag{1}$$

where Ω_{wm} is the volume of water adsorbed in the micro-pores at relative pressure $\frac{\rho_v}{\rho_v^0}$; Ω_m is the total volume of the micro-pores; n_{ads} is a material parameter, called heterogeneity factor; β_D is termed similarity constant; and $E = \beta_D E_0$ is the characteristic adsorption energy for the given system; and E_0 is the characteristic energy of adsorption for a reference vapour for which $\beta_D = 1$.

Eq. 1 can be expressed in term of water ratio by dividing both sides of the equation by the volume of solid particles Ω_s as shown in Eq. 2,

$$e_{wm} = e_m exp\left\{-\left[\frac{RT}{\beta_D E_0} ln\left(\frac{\rho_v^0}{\rho_v}\right)\right]^{n_{ads}}\right\} \tag{2}$$

where e_{wm} is the water stored in the micropores; and e_m is the microstructure void ratio.

Kelvin's equation relates the relative vapour pressure in the soil pore volume with the soil total suction (Eq. 3),

$$RH = \frac{\rho_v}{\rho_v^o} = exp\left(\frac{-sM_w}{RT\rho_w}\right) \tag{3}$$

where RH is the relative humidity, M_w is the molecular mass of water (0.018 kg/mol) and ρ_w is density of water.

Gathering the constant parameters, the following expression is finally adopted for the micro-structural water retention domain,

$$e_{wm} = e_m exp\left[-\left(C_{ads}s\right)\right]^{n_{ads}} \tag{4}$$

where n_{ads} and C_{ads} are material parameters. The parameter n_{ads} controls the curvature of the water retention curve at the high suction values. Whereas, C_{ads} is related to the original Dubinin's equation (Eq. 1) through $\beta_D E_0$, for typical values of $\beta_D E_0$ ranging between 1 and 10 kJ/mol, C_{ads} varies between 0.018 and 0.0018 MPa^{-1}.

The microstructural void ratio (e_m) in the bentonite-based materials changes during the hydration process, the evolution of the microstructure during hydration or drying process depends upon the mineralogical composition of bentonite. To account for the structural changes of the material along the water retention curve, the microstructural evolution model (Eq. 5) proposed by Della Vecchia et al. [33] is adopted in the double-structure water retention model [34].

$$e_m = e_{m0} + \beta_0 e_w + \beta_1 e_w^2 \tag{5}$$

where e_{m0} is the microstructural void ratio for the dry material $e_w = 0$ and β_0 and β_1 are parameters that quantify the swelling potential of the aggregates. Concerning the Eq. 5, it should be noted here that for high dry density and high water content, Eq. 5 may lead to values of e_m higher than the total void ratio e. In this case, it is assumed that the microstructure is completely developed and $e_m = e$.

The macrostructural water retention model is based on the capillarity in inter-aggregate pore space. The van Genuchten water retention model [38] is used to relate the macroscopic degree of saturation with the soil total suction. To describe the macroscopic water void ratio (i.e., $e_{wM} = e_M \times S_{rM}$), the macroscopic void ratio (e_M) is replaced by the $e - e_m$. In the proposed model, the Kozney-Carman law is extended for dual porosity domains in aggregated soils.

$$k = k_0 \frac{(1 - e_{M0})^M}{e_{M0}^N} \frac{e_M^N}{(1 - e_M)^M} \tag{6}$$

Additionally, based on the mercury intrusion porosimetry (MIP) data [33], the air-entry value is supposed to vary with the macroscopic void ratio (e_M) according to the relation,

$$\alpha = \frac{A}{e - e_m} \tag{7}$$

where A controls the dependence of the air-entry suction on the macrostructural void ratio (e_M).

4. Identification and calibration of model parameters

The constitutive model parameters for a fully coupled hydro-mechanical analysis can be grouped into three categories: (i) parameters related to the mechanical behavior of soil (e.g., Barcelona Basic Model parameters), (ii) parameters related to the soil water retention behavior (e.g., van Genuchten or Dieudonne water retention model) and (iii) parameters related to the hydraulic behavior (saturated and unsaturated permeability functions). The parameter selection is one of the major challenge in the coupled hydro-mechanical analysis due the lack of standard procedures for calibrating the constitutive models for unsaturated soils. In this respect, a detailed and systematic procedure is presented for identifying and calibrating the model parameters for the compacted bentonite-sand mixture from the experimental results.

4.1. Identification and calibration of BBM parameters

The calibration of the BBM presented by Alonso et al. [11] requires the selection of 10 parameters, which is quite difficult because a single parameter controls more than one aspects of soil behavior. In the present case, the suction-controlled oedometer tests were performed with the compacted samples of bentonite-sand mixture (50:50). The sample initial conditions (i.e., dry density = 1.80 Mg/m^3; water content = 9 %) were similar to the compacted blocks in the water infiltration test. Total four tests were performed with the high pressure oedometer device, which allowed to perform the test at different suction levels. The samples (dia. = 50 mm; height = 15 mm) were prepared directly inside the oedometer ring using uniaxial static compaction method.

The tests were performed in two stages i.e., the suction-equilibrium stage and the one-dimensional compression-rebound stage as depicted in Figure 4. Prior to initiate the suction-equilibrium stage, the as-compacted samples were subjected to 50 kPa surcharge pressure. Later, the vapor equilibrium technique was used to impose the desired suction level (3.39 and 10 MPa) using the saturated salt solutions. During the suction-equilibrium stage, the vertical deformation of the samples were continuously monitored . Once the sample attained the desired suction level, the second stage i.e., one-dimensional compression-rebound was initiated. For the stress-deformation characteristics of the saturated sample, the distilled water was supplied from the bottom-end under 50 kPa surcharge load prior to initiate the loading-unloading stage. For the test with as-compacted state, the sample was directly subjected to the one-dimensional compression-rebound stage.

According to the BBM [11], the yield surface corresponds to the saturated sample (i.e., $s = 0$) increases with an increase in soil suction. The rate of increase is represented by the loading-collapse curve, which is one of the fundamental characteristics of BBM. The loading-collapse curve changes it's position when the sample undergoes plastic deformation. Whereas, any combination of the net mean stress and soil suction ($p - s$) inside the elastic domain does not affect the position of loading-collapse curve (LC-curve). Hence, it is essential that the

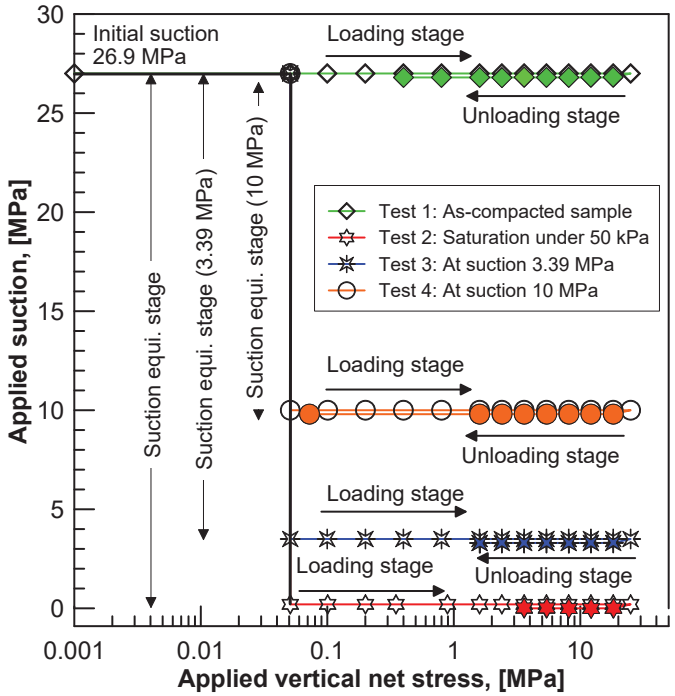

Figure 4: Stress paths for unsaturated oedometer tests on compacted sand-bentonite mixture

sample should remain in the elastic domain during the suction equilibrium-stage. In the present case, the sample was subjected to 50 kPa surcharge pressure and allowed to attain equilibrium at the imposed suction level (i.e., 3.39 or 10 MPa) under K_0 condition (Figure 4).

During the saturation, the sample was allowed to swell in the axial direction. As the swelling was not prevented, the height of the sample increased during the saturation process under the applied surcharge pressure of 50 kPa. To ensure the soil stress state (p, s) with in the elastic domain during the saturation process, the applied surcharge pressure should be lower than the expected swelling pressure of the as-compacted sample during the saturation under constant volume condition. Whereas, if the swelling is prevented at the global scale during the saturation, the stress path (p, s) may hit the yield surface in the $p-q$ plane due to the increase in net mean stress and the decrease in the apparent preconsolidation stress during the saturation process. The suction-controlled oedometer test results are shown in Figure 5 along with the deduced BBM parameters. It

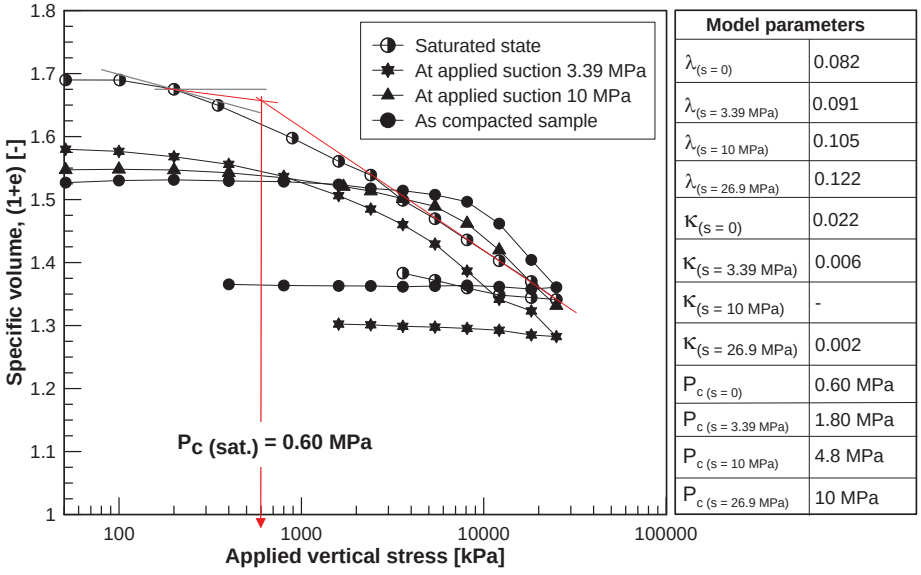

Model parameters	
$\lambda_{(s = 0)}$	0.082
$\lambda_{(s = 3.39\ MPa)}$	0.091
$\lambda_{(s = 10\ MPa)}$	0.105
$\lambda_{(s = 26.9\ MPa)}$	0.122
$\kappa_{(s = 0)}$	0.022
$\kappa_{(s = 3.39\ MPa)}$	0.006
$\kappa_{(s = 10\ MPa)}$	-
$\kappa_{(s = 26.9\ MPa)}$	0.002
$P_{c\ (s = 0)}$	0.60 MPa
$P_{c\ (s = 3.39\ MPa)}$	1.80 MPa
$P_{c\ (s = 10\ MPa)}$	4.8 MPa
$P_{c\ (s = 26.9\ MPa)}$	10 MPa

Figure 5: Suction-controlled oedometer tests results for compacted sand-bentonite mixture (50:50) with Barcelona Basic Model parameters.

should be noted here that the slope of unloading-reloading path for sample at 10 MPa applied suction is not shown in the Figure 5 due to the power failure during the test.

Alonso et al. [11] observed that the slope of normal compression lines (NCLs) for different values of soil suction decreases with increase in soil suction. In other words, the NCLs for different values of suction diverge with increasing applied stress. In the support of above statement, Alonso et al. [11] presented experimental results from Josa [39] (on compacted low plastic kaolin) and Maswoswe [40] (on compacted sandy clay). While, the oedometer test results conducted by Wheeler and Sivakumar [41] (on the compacted speswhite kaolin) revealed the converging behavior of normal compression lines under applied net mean stress levels. Wheeler et al. [17] proposed a procedure for selecting the BBM parameter values (r and p_c) to model the behavior of such soils where the NCLs converge with increasing vertical stress levels.

In the present case, the BBM parameters were selected in sequential manner.

At first, the three parameters ($\lambda(0)$, β and r), which control the slope of normal compression lines at different suction levels were determined. Figure 6a shows the predicted variation of $\lambda(s)$ with suction according to the method suggested by Wheeler et al. [17] with the r value higher than 1. In the second step, the parameters related to the elastic behavior of soil (k and k_s) were determined. The slope of the unloading/reloading line (k) is supposed to vary according to Eq. 8. Figure 6b presents the predicted variation of k with soil suction and the experimental values. It should be noted here that the fitting parameters in Figure 6b strongly conditioned by the elastic stiffness of soil in saturated condition ($s = 0$).

$$k = k_0 \left[1 + \alpha_1 s + \alpha_2 ln\left(\frac{s + u_{atm}}{u_{atm}}\right)\right] \tag{8}$$

where k_0 is the elastic stiffness in saturated conditions; α_1 and α_2 are model parameters and u_{atm} is the atmospheric pressure.

For the slope of reversible wetting-drying line (k_s), the experimental data during suction-equilibrium stage (soil suction vs. specific volume) were used. Figure 6c shows the variation of (k_s) with soil suction under 50 kPa surcharge pressure. In the last step, the parameter p_c (reference stress) were selected to match the experimental data on preconsolidation stress values at different suction levels as per the Eq. 9 proposed by Alonso et al. [11]. Figure 6d shows the loading-collapse curve for the compacted bentonite-sand mixture with the fitting parameters according to Eq. 9.

$$p_0\left(s\right) = p_c\left(\frac{p_0^*}{p_c}\right)^{\frac{\lambda(0)-k}{\lambda(s)-k}} \tag{9}$$

where $p_0\left(s\right)$ is the preconsolidation stress at soil suction (s); p_c is a reference net pressure; p_0^* preconsolidation stress for saturated condition; and k is the slope of unloading-reloading line for change in mean net stress.

The selected BBM parameters were validated against the experimental data. Figure 7 shows the predicted vs. experimental data from the suction controlled oedometer tests on the Calcigel bentonite-sand mixture (50:50). It is evident

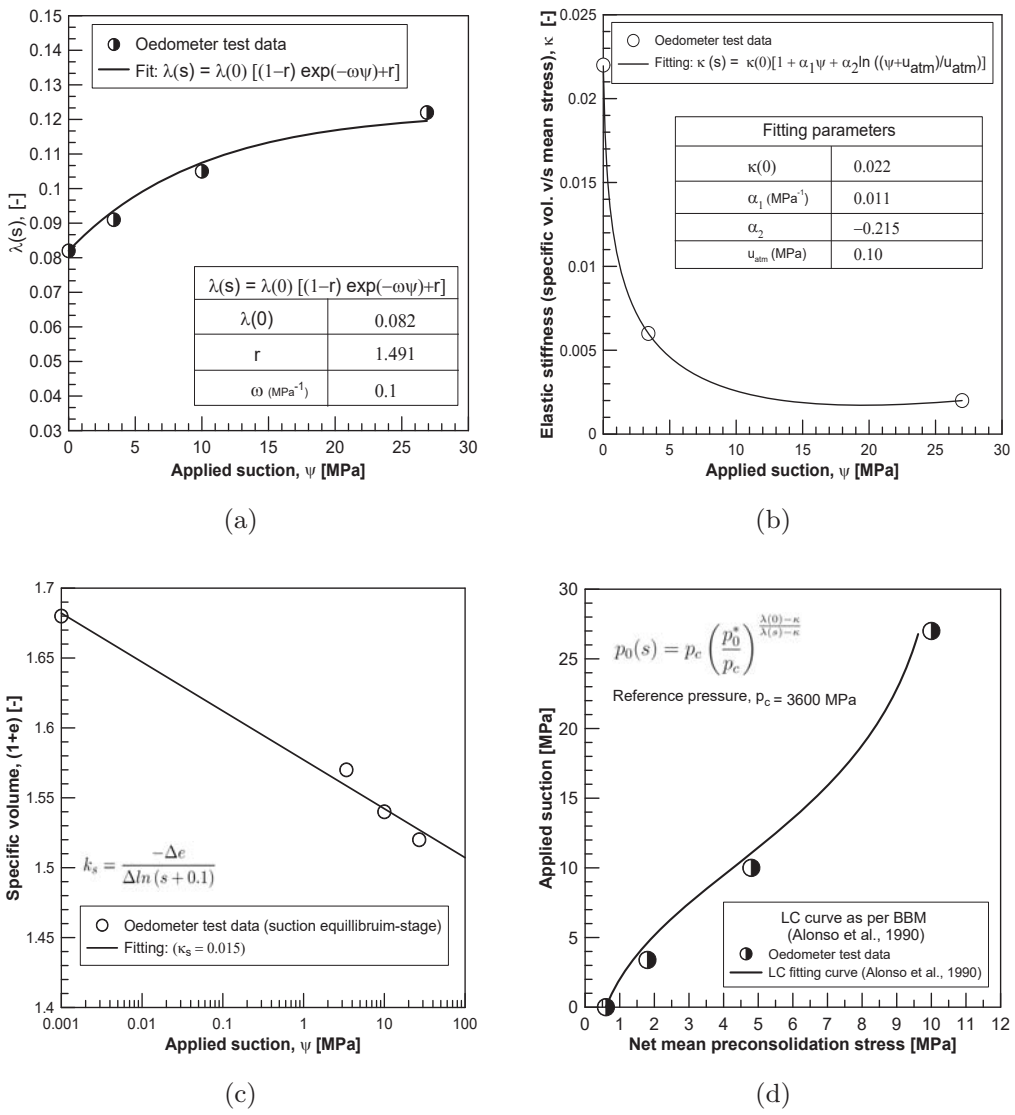

Figure 6: Determination of the BBM parameters, (a) slope of suction dependent normal compression lines, (b) applied net stress vs. specific volume at different applied suction-levels, (c) applied suction vs. specific volume at different applied net mean stress and (d) loading-collapse curve.

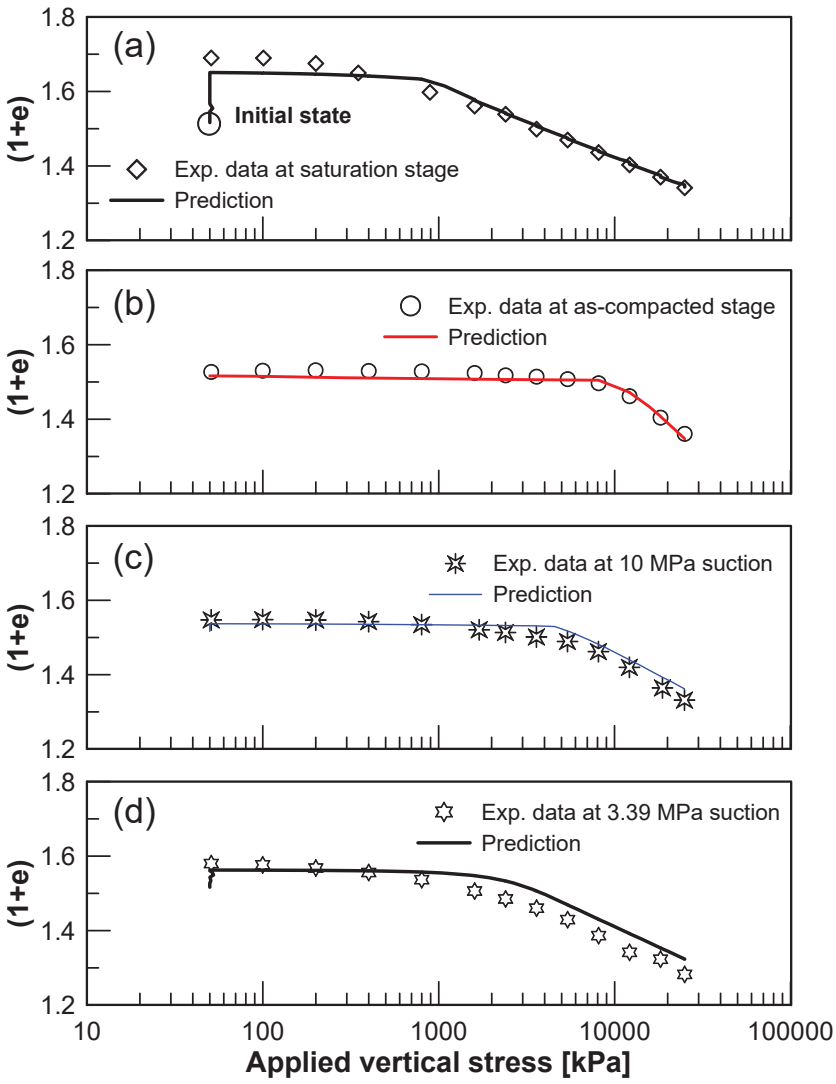

Figure 7: Validation of BBM model parameters against the suction-controlled oedometer tests.

Table 2: Barcelona Basic Model parameters for compacted sand-bentonite mixture (50:50)

Parameters	**Description**	**Value**
General parameters		
ϕ_0	Initial porosity	0.34
ρ_s (Mg.m^{-3})	Soild specific mass	2725
ψ_0 (MPa)	Inital suction	26.9
BBM plastic parameters		
$\lambda(0)$	Slope of e vs. mean stress curve for saturated conditions	0.082
p_0^* (MPa)	Preconsolidation pressure in saturated condition	0.6
p^c (MPa)	Relative reference pressure	3.6E3
r	First parameter defining the change in $\lambda(0)$ with suction	1.491
ω	Second parameter defining the change in $\lambda(0)$ with suction	0.10
BBM elastic parameters (relative to changes in stress)	$k = k_0\left[1 + \alpha_1 s + \alpha_2 ln\left(\frac{s+u_{atm}}{u_{atm}}\right)\right]$	
k_0	Initial elastic slope	0.022
α_1 (MPa^{-1})	Parameter 1 related to elastic parameter	0.011
α_2	Parameter 2 related to elastic parameter	-0.215
G (MPa)	Shear modulus (for non-linear elasticity)	23.5
BBM elastic parameter (relative to changes in suction)		
k_s	Elastic slope	0.015

from Figure 7 that the selected BBM parameters successfully predict the experimental results for both suction-equilibrium stage and the one dimensional compression stage. Table 2 summarizes the BBM parameters for compacted Calcigel bentonite-sand mixture (50:50).

4.2. Identification and calibration of double-structure water retention model parameters

The double-structure water retention model proposed by Dieudonne et al. [34] requires eight parameters, namely

- e_{m0}, β_0 and β_1 characterize the evolution of the micro-structural void ratio

(e_m) with the water ratio (e_w),

- C_{ads} and n_{ads} describe the water retention response of the intra-aggregate pores, and
- A, n, and m describe the water retention response of the inter-aggregate retention region,

The identification of model parameters related to micro-structure evolution can be estimated first, independently from the other parameters. It requires the pore size distribution (PSD) data of the compacted mixture of Calcigel bentonite-sand (50:50) at different water ratios. Additionally, the identification of e_{m0} requires the pore-size distribution of the oven-dried sample. Agus [42] obtained the PSD data from MIP tests on the sample having identical water ratio (i.e., $e_w = 0.245$). The MIP tests were conducted for the as-compacted, oven-dried and swollen sample. For the preparation of swollen sample, the as-compacted sample was allowed to swell in the axial direction only.

The MIP test data for the as-compacted sample revealed that the intra-aggregate or micro-pore volume was 59 %, while the inter-aggregate pore volume was 41 % of the total pore volume. For the oven-dried sample, the intra-aggregate pore volume was 55 %, while the inter-aggregate pore volume was 45 % of the total pore volume. For the swollen sample, the intra-aggregate pore volume was 57 %, while the inter-aggregate pore volume was 43 % of the total pore volume. Based on the above MIP test data the corresponding micro-and macro-void ratio were obtained for as-compacted samples ($e_m = 0.30$, $e_M = 0.21$ for $e_w = 0.245$), for oven-dried sample ($e_{m0} = 0.25$, $e_M = 0.20$ for $e_w = 0$) and for swollen sample ($e_{m0} = 0.45$, $e_M = 0.35$ for $e_w = 0.80$). Figure 8 shows the evolution of microstructural void ratio with the water ratio, the obtained data were fitted with the model proposed by Della Vecchia et al. [33].

In the second step, the micro-structural water retention parameters C_{ads} and n_{ads} were calibrated. The identification of these parameters requires water

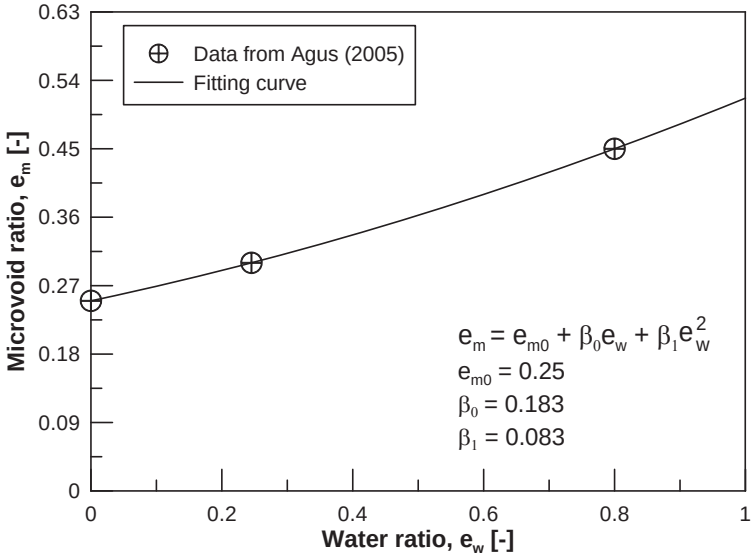

Figure 8: Evolution of micro-void ratio with water void ratio for compacted sand-Calcigel bentonite mixture (50:50) from Agus [42].

retention data for samples having different initial dry densities. In this regard, the as-compacted sample (initial dry density = 1.8 Mg/m^3) was subjected to wetting under constant volume conditions. Whereas, the water retention data for sample with 2.0 Mg/m^3 were obtained from Agus [42]. The calibration of these parameters was performed by presenting water retention data in the $(s - e_w)$ plane. At high suction values, the data point in the $(s - e_w)$ plane became independent from the sample initial dry densities. A collection of points in this place is sufficient to calibrate the two parameters.

In the final step, macro-structure water retention parameters were calibrated. The macroscopic parameter (A) allows for tracking the dependency of the air-entry suction on the void ratio: it can reproduce the correct evolution of the air-entry (or air-occlusion) value with the sample dry density. The parameters n and m control the drying-wetting rate of the material in the low suction range. Figure 9 shows the calibration of Dieudonne water retention model and the van Genuchten model against the experimental data.

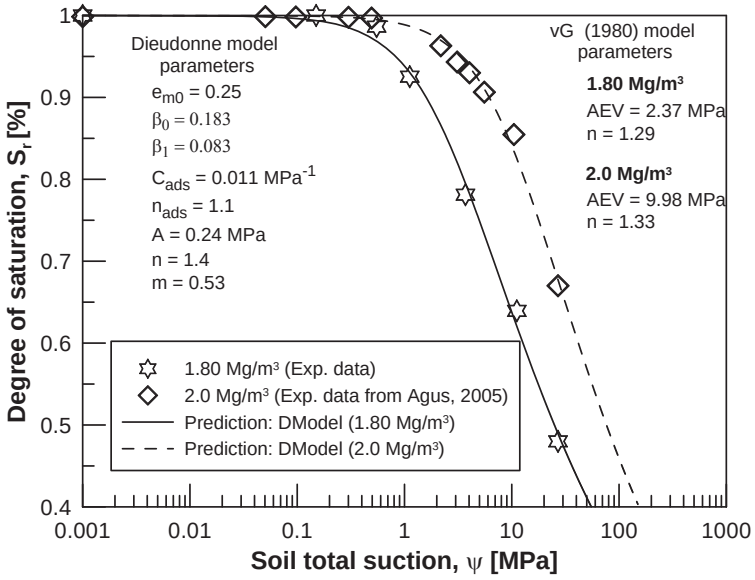

Figure 9: Calibration of water retention models against the experimental data on Calcigel bentonite-sand mixture (50:50) at two different dry densities (wetting path under confined condition).

4.3. Identification and calibration of hydraulic parameters

The saturated permeability of the Calcigel bentonite-sand mixture (50:50) was determined by conducting a falling head permeability test in the oedometer. Prior to conduct the test, the as-compacted sample (initial density = 1.8 Mg/m^3; water content = 9 %) was subjected to hydration under constant volume condition. Once the sample got saturation, the top inlet was connected to a manometer tube, while the bottom inlet was connect to the volume pressure controller for applying the water pressure and calculating the flow rate. Later, the saturated permeability was calculated. The identification of Kozeny-Carman [43, 44] saturated permeability model (Eq. 10) parameters requires the saturated permeability values at different initial porosity values. These values were obtained from Agus [42] (sample initial dry density = 2.0 Mg/m^3; water content = 9 %) and Long [45] (sample initial dry density = 1.4 Mg/m^3; water content = 9 %) on the similar bentonite-sand mixture (50:50).

$$K = K_0 \frac{(1-\phi_0)^m}{\phi_0^n} \frac{\phi^n}{(1-\phi)^m} \tag{10}$$

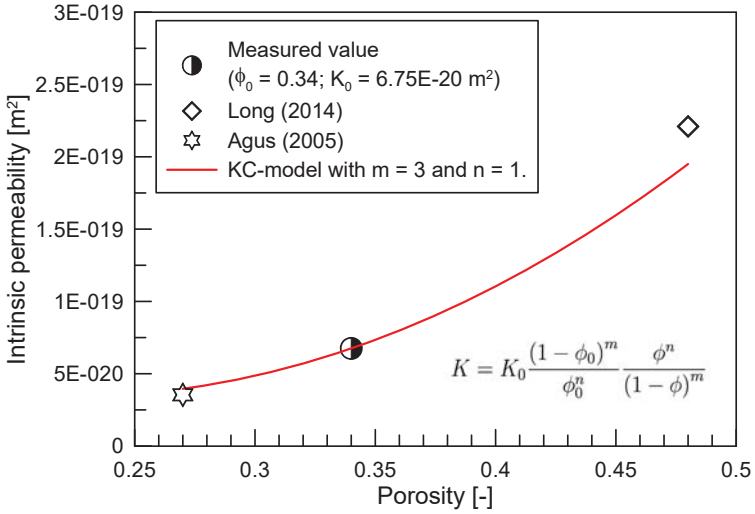

Figure 10: Sample initial porosity versus intrinsic permeability of compacted Calcigel bentonite-sand mixture (50:50): experimental data and the predicted values using Kozeny-Carman model.

where, K is intrinsic permeability (m^2) of material with porosity ϕ, K_0 is intrinsic permeability (m^2) of material with reference porosity ϕ_0, m and n are fitting parameter.

The intrinsic permeability (m^2) of material is related with the saturated permeability of material (m/s) as shown by Eq. 11.

$$k_f = \frac{K_f . \rho_f . g}{\mu_f} \tag{11}$$

where, k_f is the saturated permeability (m/s), K_f is intrinsic permeability (m^2) of material, ρ_f is the density of fluid (kg/m^3), g is the coefficient of gravity (m/s^2) and μ_f is the dynamic viscosity of fluid (Pa.s).

The collected and measured saturated permeability data with the Kozeny-Carman model parameters for Calcigel bentonite-sand mixture are shown in Figure 10. The unsaturated coefficient of permeability versus suction (i.e., the unsaturated permeability function) was computed from the saturated coefficient of permeability and wetting curve through [38]. Table 3 summarizes the water retention parameters and the hydraulic parameters for compacted Calcigel bentonite-sand mixture.

Table 3: Hydraulic parameters for compacted sand- Calcigel bentonite mixture having equal dry mass ratio.

Parameters	**Description**	**Value**
van Genuchten (1980) model	$S_e = \left(1 + \left(\frac{s}{A}\right)^n\right)^{-\left(1-\frac{1}{n}\right)}$	
A (MPa)	Air-entry suction	2.37
n	Shape function for retention curve	1.29
S_{max}	Max. field saturation	1
S_{res}	Residual field saturation	0
Dieudonne et al. (2017): Microstructure water retention model	$e_m = e_{m0} + \beta_0 e_w + \beta_1 e_w^2$ $e_{wm} = e_m exp\left[-\left(C_{ads} s\right)\right]^{n_{ads}}$	
e_{m0}	Micro void ratio at $e_w = 0$	0.25
β_0	Parameter 1 for microstructure evolution	0.183
β_1	Parameter 2 for microstructure evolution	0.083
C_{ads} $(\text{MPa})^{-1}$	Parameter 1 for adsorption (Micro-level)	11.0E-3
n_{ads}	Parameter 2 for adsorption (Micro-level)	1.1
Dieudonne et al. (2017): Macrostructure water retention model	$e_{wM}\left(s, e, e_m\right) = \left(e - e_m\right)\left[1 + \left(\frac{s}{\alpha}\right)^n\right]^{-m}$	
$\alpha = \frac{A}{e - e_m}$ (MPa)	A (Macro-level parameter)	0.24
m	Shape parameter 1 for retention curve	0.53
n	Shape parameter 2 for retention curve	1.4
Kozney-Carman formulation	$K = K_0 \frac{(1-\phi_0)^m}{\phi_0^n} \frac{\phi^n}{(1-\phi)^m}$ for vG model $K = K_0 \frac{(1-e_{M0})^m}{e_{M0}^n} \frac{e_M^n}{(1-e_M)^m}$ for Dieudonne model	
K_0 (m^2)	Intrinsic permeability with matrix ϕ_0 or e_{M0}	6.75E-20
K (m^2)	Intrinsic permeability with matrix ϕ or e_M	-
m	Parameter 1 for KC formulation	3
n	Parameter 2 for KC formulation	1
Relative permeability (water/air)	$k_{rw} = \sqrt{S_{rw}}\left(1 - \left(1 - S_{rw}^{\frac{1}{\lambda}}\right)^{\lambda}\right)^2$	
n	Parameter for water/air relative permeability	0.5

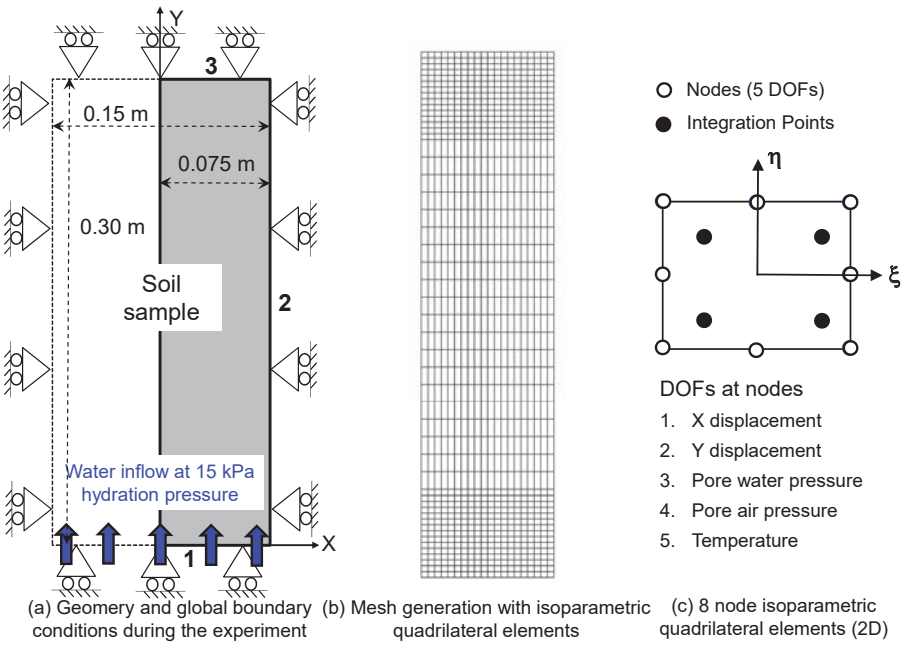

Figure 11: Features of numerical simulation, (a) geometry with global force and displacement boundary conditions during the experimental investigations, (b) mesh formation with 2D 8 nodes isoparametric quadrilateral elements and (c) 2D isoparametric quadrilateral element with 5 degree of freedoms.

5. Features of numerical simulation

A 2D axisymmetric model along Y-axis is selected for a fully coupled hydro-mechanical analysis. The model dimensions were selected according to the sample size in the water infiltration test (dimension along X-axis = 75 mm; dimension along Y-axis = 300 mm). The model geometry and initial boundary conditions are shown in Figure 11.

The initial total stress in the material was assumed to be isotropic and equal to the 0.1 MPa. An isoparametric quadrilateral element (2D) with 8 nodes was selected for the analysis. The element for 2D case posses five degrees of freedom at each node: two displacements of the soil skeleton, a liquid water pressure, a gas (dry air+vapor) pressure and temperature. The temperature is

kept constant at 20 °C. The initial total suction of the material was assigned as 26.90 MPa. It was assumed that the contact between the sample and the cell is frictionless. The hydration-pressure (i.e., 15 kPa) was applied by increasing the initial pore water pressure of the bottom nodes.

6. Results and discussion

The water infiltration test results highlighted the characteristics features of the coupled hydro-mechanical behavior of compacted bentonite-sand mixture. A fully coupled hydro-mechanical analysis was performed for predicting the water infiltration test results. The simulation results are presented and discussed in three subsections, such as:

- Evolution of state variables,
- Material swelling behavior, and
- Soil water retention behavior.

6.1. Evolution of state variables

Figure 12 shows the comparison between the predicted and measured relative humidity values over time along the height of soil sample. The predicted values using van Genuchten and Dieudonne soil water retention model show a good agreement with the experimental values. However, a minor variation can be observed in the predicted and measured values for the measurement sections X2 and X3.

Figure 13 shows the comparison between the predicted and measured water content over time for measurement sections X1, X2 and X3. Similar to the relative humidity evolution, the effect of distance on the saturation rate is evident. Likewise, the relative humidity evolution at section X1, the water content increases rapidly with the initiation of hydration. The predicted values at section X1 agree well with the experimental results. The predicted values

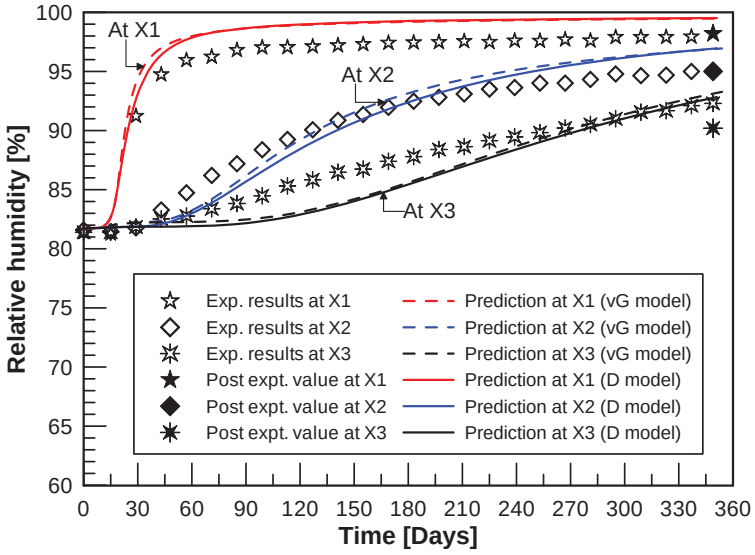

Figure 12: Experimental vs. simulation results: elapsed time vs. relative humidity values along the height of soil sample.

using Dieudonne water retention model showed a better agreement with the experimental values at measurement section X2 and X3. However, the predicted values of water content were slightly higher than the measured ones.

The predicted water volume infiltrated into the soil sample was compared with the measured volume during the water infiltration test (Fig. 14). The figure also shows the calculated volume which infiltrated into the soil sample deduced from the transient water content measurements. The predicted values shows a good agreement with the measured and calculated water volume with some minor variations. A decrease in the flow rate with the elapsed is evident from the Figure 14, which signifies the effect of water potential gradient along the height of soil sample on the rate of saturation.

The Kozney-Carman (KC) equation [43, 44] for the porosity dependent saturated hydraulic conductivity along with the Mualem-van genuchten equation [38] provide a good estimation of material unsaturated hydraulic conductivity during the hydration process. The Mualem-van genuchten closed form equation for unsaturated hydraulic conductivity function (k_{rl}) is a non-linear function of degree of saturation (S_r), which was calculated using the van Genuchten [38]

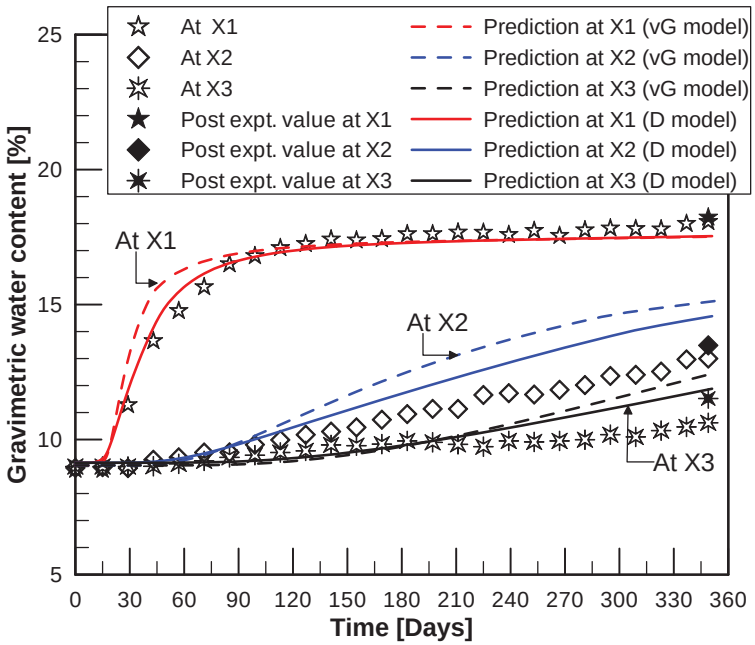

Figure 13: Experimental vs. simulation results: elapsed time vs. water content along the height of soil sample.

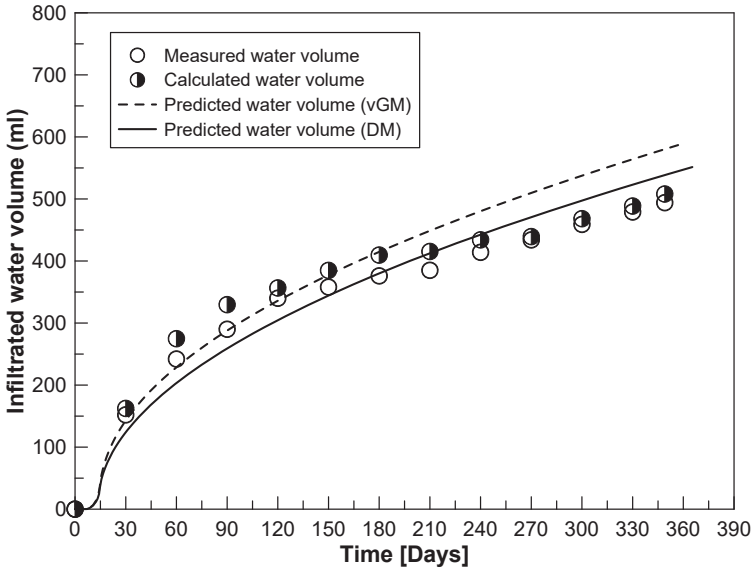

Figure 14: Experimental vs. simulation results: elapsed time vs. infiltrated water volume.

and Dieudonne soil water retention model [34].

The original Kozeny-Carman equation [43, 44] does not consider the dual porosity domains in the compacted bentonite-based materials. Whereas, the equation is modified for relating water permeability to the macrostructural void ratio e_M or macroporosity ϕ_M in the Dieudonne water retention model based on the assumption that water flow takes place essentially in the macropores (see Eq. 6). The progressive saturation of the material induces the void ratio change as depicted in Figure 15a. The initiation of hydration from the bottom-end increase the void ratio at section X1 close to hydration end. Since the global swelling of the sample is kept constant, the increase of porosity at the bottom of the sample should be counterbalanced by an increase of porosity at the measurement sections X2 and X3. Accordingly, the upper part of the sample is compressed by the swollen bottom part.

According to the Dieudonne water retention model, the micro void ratio (e_m, initial value = 0.30) increases with increase in water content or decrease in soil total suction during the hydration process (Fig. 15b). As the macro void ratio (e_M) is defined as the difference between the total void ratio e and the microstructural void ratio e_m. Hence, the macro void ratio progressively decreases during the hydration process, which results into the reduction in the saturated water permeability according to KC equation as depicted in Figure 16a. The evolution unsaturated hydraulic conductivity shown in Figure 16b. It is evident from Figure 16b that the van Genuchten model [38] provides slightly higher unsaturated hydraulic conductivity values than the Dieudonne model [34]. Consequently, the predicted values (i.e., relative humidity, water content and flow rate) also show some minor variations as depicted in Figures 12, 13 and 14. In general both the models are capable to capture the water transfer mechanism and the permeability evolution in the compacted bentonite sand mixture during the hydration process under constant volume condition.

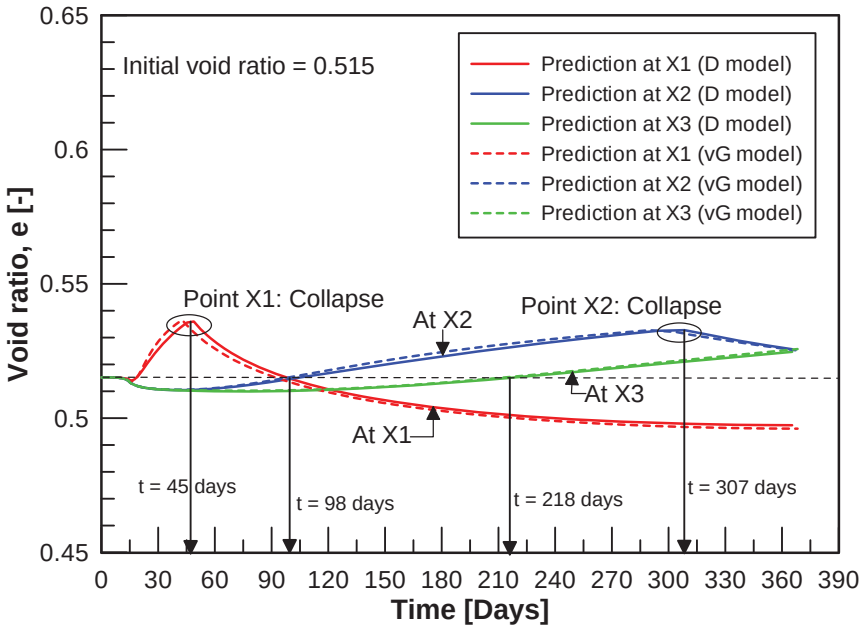

(a)

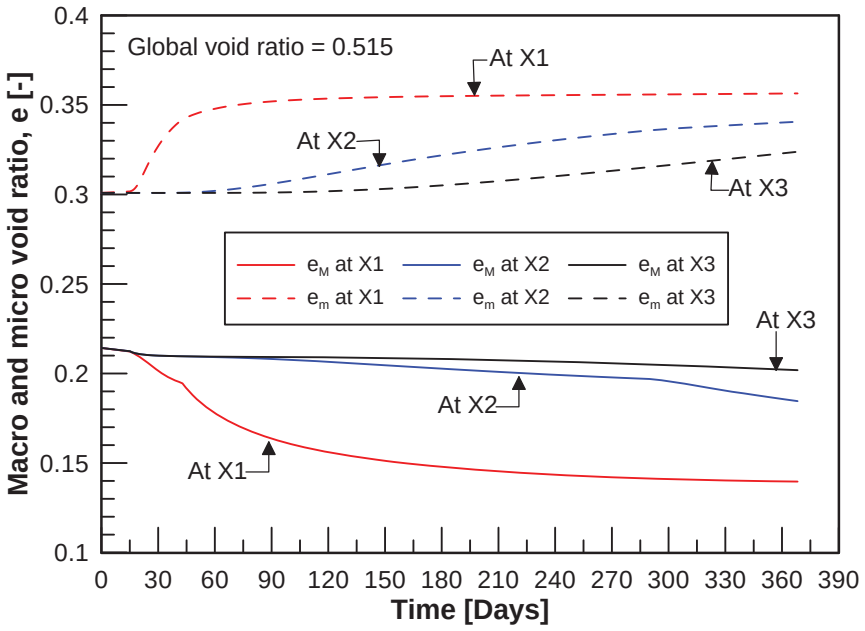

(b)

Figure 15: Numerical simulation results (a) evolution of void ratio and (b) evolution of micro and macro void ratio according to Dieudonne water retention model [34].

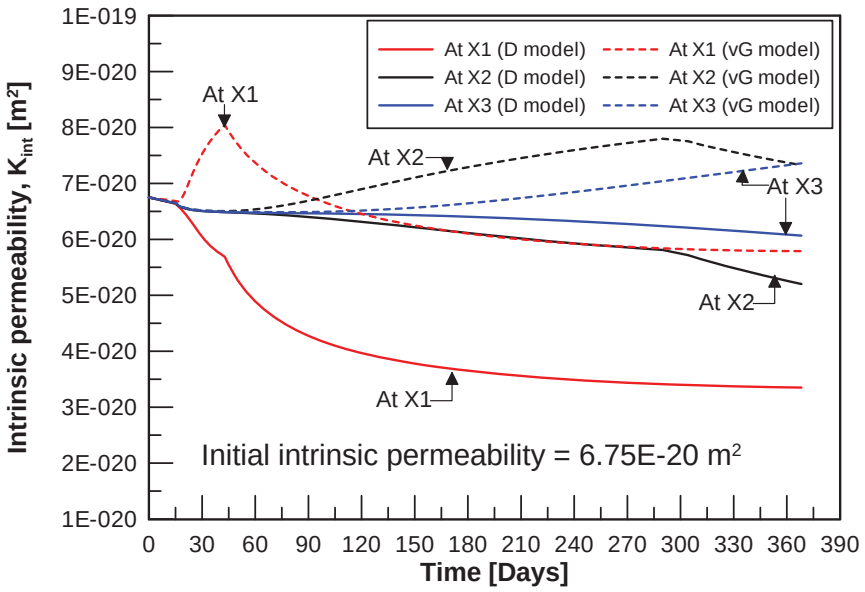

(a)

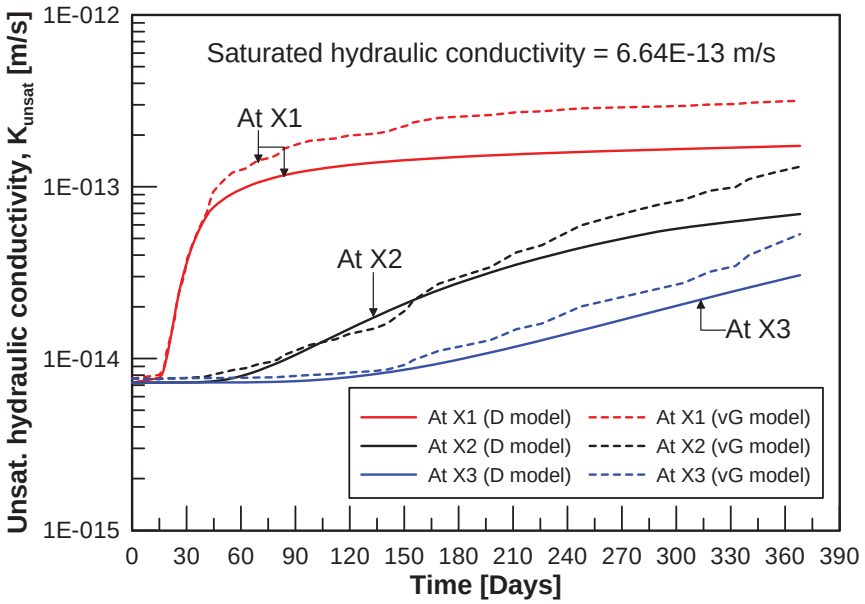

(b)

Figure 16: Numerical simulation results (a) evolution of intrinsic permeability (m^2) and (b) evolution of hydraulic conductivity (m/s) over time for measurement section X1, X2 and X3.

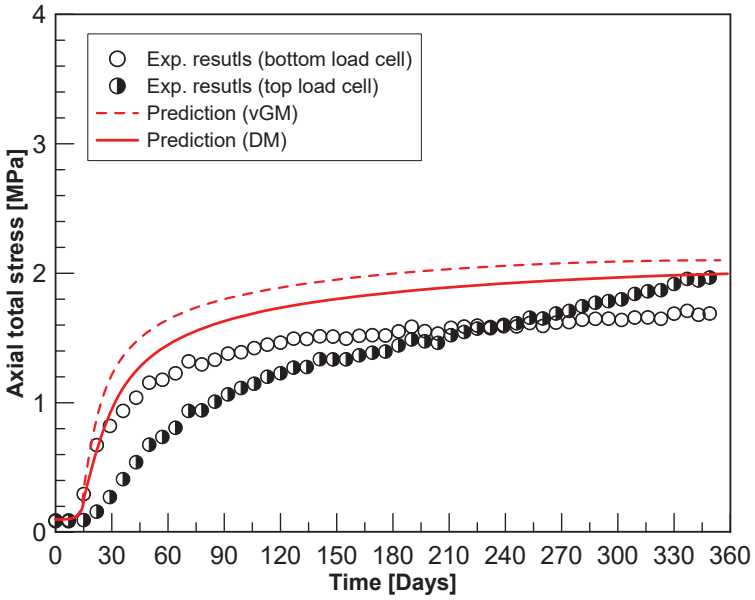

Figure 17: Experimental vs. simulation results: elapsed time vs. axial total stress.

6.2. Material swelling behavior

The comparison between the predicted and measured axial total stress at the top and bottom ends are presented in Figure 17. The top load cell measured the applied stress from the bottom elements during the hydration process. Under confined condition and at equilibrium, it may be anticipated that the measured axial stress at both ends of the sample are equal. However, it was observed that the axial stress developed at the top end of the sample was not transmitted towards the bottom of the sample. This can be attributed to the following factors, such as (i) dissimilar compressibility characteristics along the height of the sample due to the difference in the water content along the height, (ii) the presence of construction joints meant for installing the pressure transducers, (iii) the side frictional resistance between the sample and the PVDF rings, and (iv) the composite nature of the sample due to the presence of sensors that created complex stress-deformation characteristics of the system. These features were not considered during the simulation. However, a decent agreement can be observed between the experimental values and the model predictions at the bottom end. The development of axial total stress at the bottom end exhibits

a rapid increase before reaching to 1.1 MPa in 45 days. With the elapsed time, the axial swelling pressure at the bottom end increased gradually and reached to 1.68 MPa in 349 days. The simulation results successfully captured the trend, however the predicted values were slightly higher than the experimental measurements.

Figure 18 presents the comparison between the predicted and measured values of lateral swelling pressure for the measurement sections X1, X2 and X3. During the experiment, the lateral swelling pressure measurements were performed with the cylindrical-piston and a miniature load cell assembly (see Figure 2). These PVDF pistons were kept in direct contact with the soil sample during the installation of test-setup. As soon as the hydration started, the lateral total stress measurement system at the section X1 responded quickly and reached to 2.18 MPa within 45 days. With the further hydration, the measured values at the section X1 showed some oscillations before reaching to a value of 2.13 MPa within 349 days. The model predictions showed a good agreement with the experimental values at section X1. However, the numerical simulation did not reproduce the experimental data for measurement sections X2 and X3.

In further analysis, Figure 19a presents the variation in the saturated preconsolidation pressure with the soil suction for the measurement sections X1, X2 and X3. The yielding/collapse at section X1 and X2 along with the increase in preconsolidation stress in saturated state is evident at sections X1 and X2. While the stress-state at section X3 ($p - s$) varies within the elastic domain of LC curve. Figure 19b shows the evolution of LC curve along the height of soil sample, the data were obtained from the numerical analysis. Additionally, the oedometer tests data were also shown. The elastoplastic behavior of material at the measurement sections X1 and X2 and resulting increase in the preconsolidation pressure (i.e., isotropic hardening) can be observed from Figure 19b.Whereas, the material at the section X3 exhibited the elastic swelling. Hence, the experimental results along with the numerical analysis indicated that the material stress-state in $p - s$ plane evolves in elastic to elastoplastic domain during the hydration process.

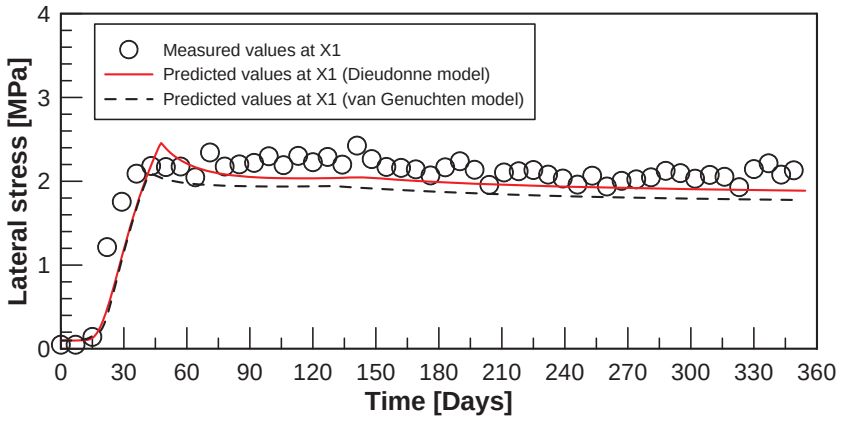

(a) At section X1

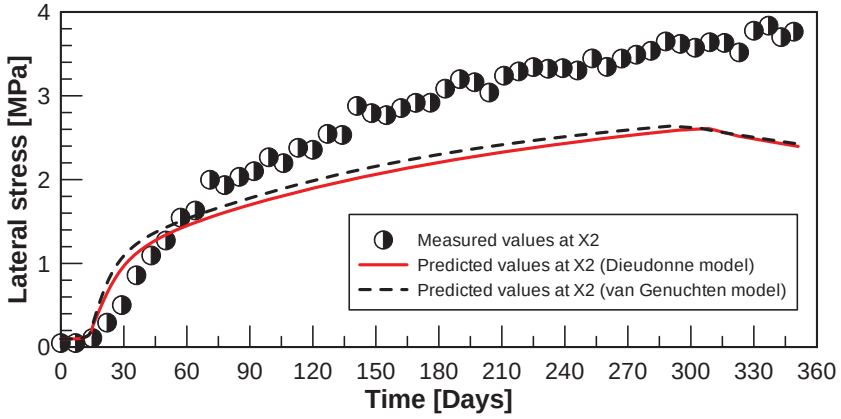

(b) At section X2

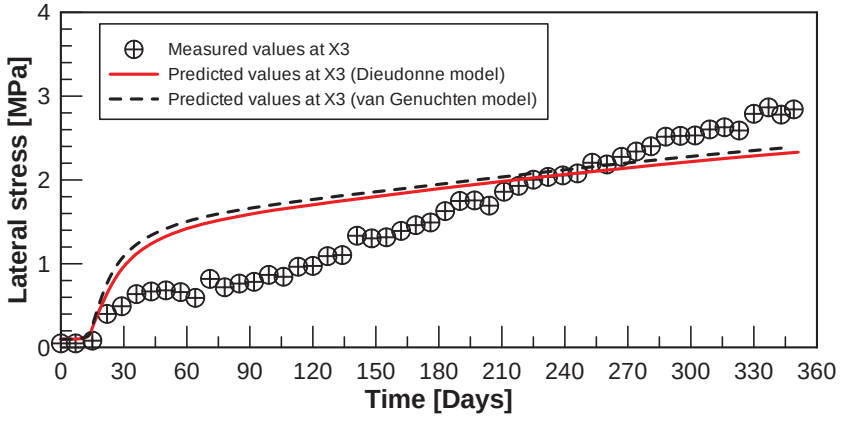

(c) At section X3

Figure 18: Experimental vs. simulation results: elapsed time vs. lateral total stress.

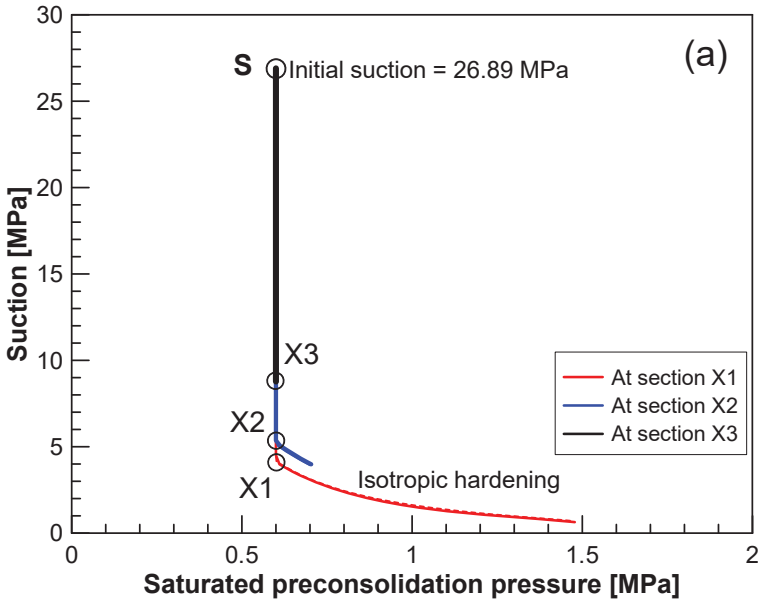

(a)

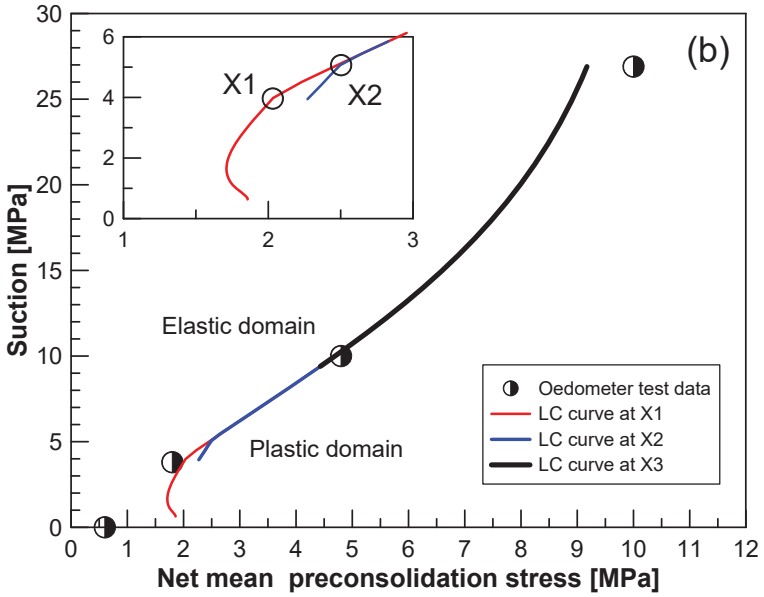

(b)

Figure 19: Numerical simulation results (a) saturated preconsolidation stress vs. soil suction and (b) evolution of loading-collapse curve along the sample height.

Since the sample was laterally and axially confined in the numerical analysis, its total volume remained constant during the hydration process. However the local porosity variations can be observed, which lead to a heterogeneous distribution of permeability. Under the confined condition, the elastic strains according to the Barcelona basic model is defined as:

$$d\varepsilon_v^e = d\varepsilon_{vp}^e + d\varepsilon_{vs}^e = \frac{k}{1+e}\frac{dp}{p} + \frac{k_s}{1+e}\frac{ds}{s+u_{atm}} = \frac{dp}{K} + \frac{ds}{K_s} \tag{12}$$

For constant volume condition:

$$d\varepsilon_v^e = 0 \tag{13}$$

Hence,

$$d\varepsilon_{vp}^e = -d\varepsilon_{vs}^e \tag{14}$$

and

$$\frac{dp}{K} = -\frac{ds}{K_s} \tag{15}$$

$$\frac{k}{1+e}\frac{dp}{p} = -\frac{k_s}{1+e}\frac{ds}{s+u_{atm}} \tag{16}$$

$$dp = -\frac{k_s}{k}\frac{ds}{(s+u_{atm})}.p \tag{17}$$

The incremental change in the magnitude of net mean stress in the BBM elastic domain is isotropic and can be calculated using Eq. 17 under the confined swelling condition. Eq. 17 indicates that the incremental change in the magnitude of net mean stress depends on the ratio of elastic stiffness $\left(\frac{k_s}{k}\right)$, incremental change in soil suction (ds) and the current stress state (p) and suction. According to Figure 18, the incremental rate of radial total stress was the same for the measurement sections X2 and X3 during the initial phase of hydration. It was mainly due to the insignificant change in the soil suction at X2 and X3 during the initial phase of hydration (i.e., 45 days). After 45 days, the suction at X2 decreases faster than the section X3, so the radial stress at section X2 deviates from section X3. The radial total stress evolution at section X2 exhibit collapse behavior at time t = 300 days. Hence, the experimental results

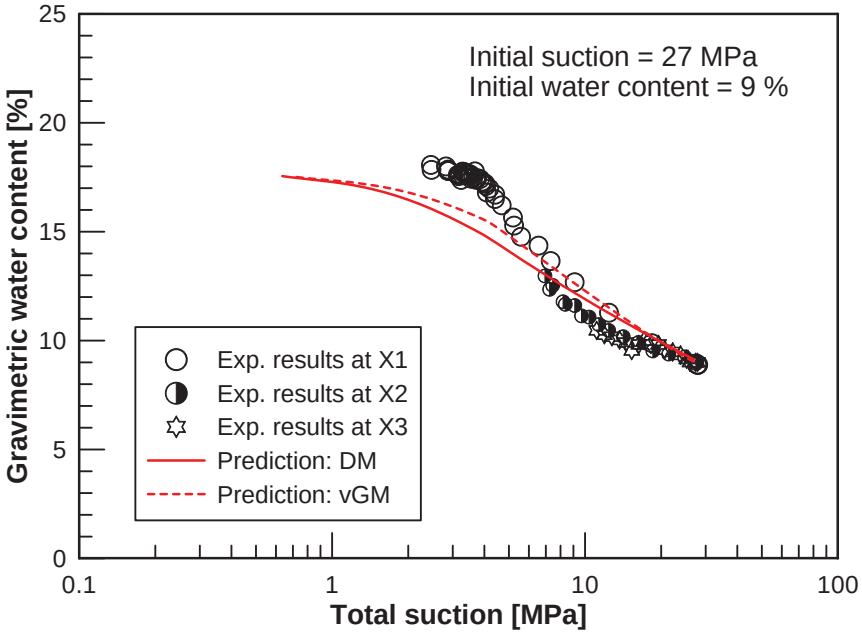

along with the numerical analysis indicate that the material stress-state in $p-s$ plane evolves in elastic to elastoplastic domain under the influence of coupled processes such as saturation-rate and soil current stress state (p, s) along with the current-ratio of elastic stiffness $\left(\frac{k_s}{k}\right)$.

In general, the swelling behavior of compacted bentonite-sand mixture during the hydration from one end involves various complex processes, such as soil swelling, interaction between different soil layers and non-uniform changes in the sample condition during the progressive hydration process. Additionally, the presence of technical/constructional gaps and non-uniform soil stiffness along the height of soil sample during the heterogeneous hydration process are also responsible for a different axial and lateral swelling pressure dynamics.

6.3. Soil water retention behavior

Figure 6.3 compares the predicted and measured data (soil suction vs. transient gravimetric water content). The simulation results exhibited a unique relationship along the sample height and showed good agreement with the experimental values within the range of initial suction (27 MPa) to 7 MPa. In the numerical simulation, the water content values are calculated from the updated

void ratio and the current degree of saturation (S_r) obtained from $s - S_r$ relationship according to van Genuchten or Dieudonne water retention model. For the lower suction range (i.e., RH $\geq$ 95%), the predicted values slightly deviate from the experimental results and underestimate the water content.

7. Conclusions

Numerical simulation of water infiltration test was conducted with finite element code LAGAMINE. As an reference case, Barcelona Basic Model [11] for describing the mechanical behavior of unsaturated expansive soils was adopted along with the recently developed soil water retention model based on clay micro structural features in compacted state [34]. The simulation results were compared with classical soil water retention model [38].

As a key ingredient of original BBM formulation as proposed by [11], soil suction is treated as hardening parameter. Hence, the compression index (λ) decreases with an increase in soil suction. While the suction controlled oedometer tests revealed that the soil compression index (λ) first diverge and then converge for corresponding lower and higher values of applied net mean vertical stress. The BBM parameters were identified and calibrated using the suction-controlled oedometer test results as per the procedure described by [17]. The simulation results for suction-controlled oedometer tests showed a good agreement with experimental results. The model parameters pertaining to soil water retention behavior were identified and calibrated with the multistage wetting tests under constant volume condition using isochoric cell.

The simulation results showed a good agreement with the observed experimental data pertaining to the evolution of water content and relative humidity and captured the water transfer mechanism and the permeability evolution in the compacted bentonite sand mixture during the transient hydration process. Considering the mechanical behavior, the modified BBM was able to predict the measured axial total stress evolution at the bottom end in both qualitative and quantitative manner. The anisotropy in material properties were not considered

in the conventional formulation proposed by [11]. However, it was interesting to see that the simulation results successfully predicted the experimental measurements of axial and lateral total stress close to the hydration end. While for the inner sections (i.e., X2 and X3), the model predictions showed some disagreement with the measured lateral total stress. The experimental investigations highlighted the presence of inter-facial friction/cohesion between the soil sample and cell wall and it's effect on the total stress transfer towards the material inner sections. In common practice, the inter-facial friction between the soil sample and the cell wall is not considered during the numerical simulation. It is not only the anisotropy in fabric, other factors such as presence of technical/constructional gaps, different swelling scenarios/stress-volume paths and non-uniform soil stiffness along the height of soil sample are also responsible for a different axial and lateral swelling pressure dynamics.

References

[1] T. Rothfuchs, N. Jockwer, R. Miehe, C. L. Zhang, Self-sealing barriers of clay/mineral mixtures in a clay repository: Sb experiment in the mont terri rock laboratory, Tech. rep., Gesellschaft für Anlagen-und Reaktorsicherheit (GRS) (2005).

[2] M. Jobmann, J. Flügge, J. Hammer, P. Herold, J. Krone, T. Kühnlenz, S. Li, A. Lommerzheim, A. Meleshyn, J. Wolf, Site-specific evaluation of safety issues for high-level waste disposal in crystalline rocks, Tech. rep., GRS BGR DBE TEC (2015).

[3] M. Jobmann, J. Flügge, R. Gazul, J. Hammer, P. Herold, J. Krone, E. Kuate Simo, T. Kühnlenz, E. Laggiard, A. Lommerzheim, A. Meleshyn, C. Müller, A. Rübel, J. Wolf, H. Zhao, Investigation on long-term safety aspects of a radioactive waste repository in a diagenetic clay formation, Tech. rep., GRS BGR DBE TEC (2017).

[4] E. Alonso, J. Alcoverro, F. Coste, L. Malinsky, V. Merrien-Soukatchoff,

I. Kadiri, T. Nowak, H. Shao, T. Nguyen, A. Selvadurai, et al., The febex benchmark test: case definition and comparison of modelling approaches, International Journal of Rock Mechanics and Mining Sciences 5 (42) (2005) 611–638.

[5] A. Gens, M. Sánchez, L. D. N. Guimarães, E. Alonso, A. Lloret, S. Olivella, M. Villar, F. Huertas, A full-scale in situ heating test for high-level nuclear waste disposal: observations, analysis and interpretation, Géotechnique 59 (4) (2009) 377–399.

[6] M. Villar, R. Campos, L. Gutiérrez-Nebot, Long-term performance of engineered barrier systems pebs, EB experiment Laboratory post-mortem analyses report, the Seventh Framework Programme of the European Atomic Energy Community (Euratom), DELIVERABLE (D2.1-7) (2014) 1–34.

[7] P. Martin, J. Barcala, Large scale buffer material test: Mock-up experiment at ciemat, Engineering Geology 81 (3) (2005) 298–316.

[8] M. Villar, J. García-Siñeriz, I. Bárcena, A. Lloret, State of the bentonite barrier after five years operation of an in situ test simulating a high level radioactive waste repository, Engineering geology 80 (3-4) (2005) 175–198.

[9] S. Saba, Y.-J. Cui, J.-D. Barnichon, A. M. Tang, Investigation of the swelling behaviour of compacted bentonite–sand mixture by mock-up tests, Canadian Geotechnical Journal 51 (12) (2014) 1399–1412.

[10] S. Tripathy, H. R. Thomas, R. Bag, Geoenvironmental application of bentonites in underground disposal of nuclear waste: Characterization and laboratory tests, Journal of Hazardous, Toxic, and Radioactive Waste 21 (1) (2015) D4015002.

[11] E. E. Alonso, A. Gens, A. Josa, A constitutive model for partially saturated soils, Géotechnique. 40 (3) (1990) 405–430.

[12] K. Roscoe, J. Burland, On the generalised stress-strain behaviour of wet clay, Engineering Plasticity (1968) 535–609.

[13] C. H. Delahaye, E. Alonso, Soil heterogeneity and preferential paths for gas migration, Engineering geology 64 (2-3) (2002) 251–271.

[14] J. Vaunat, A. Gens, Analysis of the hydration of a bentonite seal in a deep radioactive waste repository, Engineering geology 81 (3) (2005) 317–328.

[15] M. T. Zandarin, E. Alonso, S. Olivella, A constitutive law for rock joints considering the effects of suction and roughness on strength parameters, International Journal of Rock Mechanics and Mining Sciences 60 (2013) 333–344.

[16] M. Sánchez, A. Gens, S. Olivella, Thm analysis of a large-scale heating test incorporating material fabric changes, International Journal for Numerical and Analytical Methods in Geomechanics 36 (4) (2012) 391–421.

[17] S. Wheeler, D. Gallipoli, M. Karstunen, Comments on use of the barcelona basic model for unsaturated soils, International journal for numerical and analytical methods in Geomechanics 26 (15) (2002) 1561–1571.

[18] D. Gallipoli, F. DOnza, S. J. Wheeler, A sequential method for selecting parameter values in the barcelona basic model, Canadian Geotechnical Journal 47 (11) 1175–1186.

[19] F. DOnza, D. Gallipoli, S. J. Wheeler, A new procedure for determining parameter values in the barcelona basic model, in: Unsaturated Soils: Research and Applications, Springer, 2012, pp. 93–102.

[20] D. Gallipoli, F. D'Onza, Calibration of elasto-plastic models for unsaturated soils under isotropic stresses, Engineering Geology 165 (2013) 64–72.

[21] R. N. Brooks, A. T. Corey, Hydraulic properties of porous media, Colorado State University, Hydro Paper 3 (1964) 27.

[22] M. T. van Genuchten, A closed-form equation for predicting the hydraulic conductivity of unsaturated soils1, Soil Sci. Soc. Am. J. 44 (1980) 892–898.

[23] D. Fredlund, A. Xing, Equation for the soil-water characteristic curve, Can. Geotech. J. 31 (1994) 521–532.

[24] D. Gallipoli, A. Gens, R. Sharma, J. Vaunat, An elasto-plastic model for unsaturated soil incorporating the effects of suction and degree of saturation on mechanical behaviour, Géotechnique 53 (1) (2003) 123–135.

[25] M. Nuth, L. Laloui, Advances in modelling hysteretic water retention curve in deformable soils, Computers and Geotechnics 35 (6) (2008) 835–844.

[26] A. Tarantino, A water retention model for deformable soils, Géotechnique 59 (9) (2009) 751–762.

[27] D. Mašín, Predicting the dependency of a degree of saturation on void ratio and suction using effective stress principle for unsaturated soils, International Journal for Numerical and Analytical Methods in Geomechanics 34 (1) (2010) 73–90.

[28] D. Gallipoli, A hysteretic soil-water retention model accounting for cyclic variations of suction and void ratio, Geotechnique 62 (7) (2012) 605–616.

[29] Y. Cui, C. Loiseau, P. Delage, Microstructure changes of a confined swelling soil due to suction controlled hydration, in: Proceedings of the 3rd International Conference on Unsaturated Soils (UNSAT 2002), Recife, Brésil. Sous la direction de J. FT Jucá, TMP de Campos et FAM Marinho, Vol. 2, 2002, pp. 593–598.

[30] A. Lloret, M. V. Villar, M. Sanchez, A. Gens, X. Pintado, E. E. Alonso, Mechanical behaviour of heavily compacted bentonite under high suction changes, Géotechnique. 53 (1) (2003) 27–40.

[31] P. Delage, D. Marcial, Y. J. Cui, X. Ruiz, Ageing effects in a compacted bentonite: a microstructure approach, Géotechnique. 56 (5) (2006) 291–304.

[32] E. Romero, J. Vaunat, Retention curves of deformable clays, in: In Proceedings of the international workshop on unsaturated soils, CRC Press, 2000, pp. 91–106.

[33] G. Della Vecchia, A.-C. Dieudonné, C. Jommi, R. Charlier, Accounting for evolving pore size distribution in water retention models for compacted clays, International Journal for Numerical and Analytical Methods in Geomechanics 39 (2015) 702–723.

[34] A.-C. Dieudonne, G. Della Vecchia, R. Charlier, Water retention model for compacted bentonites, Canadian Geotechnical Journal 54 (7) (2017) 915–925.

[35] DIN18123, Soil, investigation and testing - determination of grain-size distribution (11 1996).

[36] F. Collin, X.-L. Li, J.-P. Radu, R. Charlier, Thermo-hydro-mechanical coupling in clay barriers, Engineering Geology 64 (2-3) (2002) 179–193.

[37] M. Dubinin, L. Radushkevich, The equation of the characteristic curve of the activated charcoal, in: Proceedings of the Union of Soviet Socialist Republics Academy of Sciences, Vol. 55, 1947, pp. 331–337.

[38] M. T. Van Genuchten, A closed-form equation for predicting the hydraulic conductivity of unsaturated soils 1, Soil science society of America journal 44 (5) (1980) 892–898.

[39] A. J. García-Tornel, Un modelo elastoplástico para suelos no saturados, Ph.D. thesis, Universitat Politècnica de Catalunya (1988).

[40] J. Maswoswe, Stress paths for compacted soil during collapse due to wetting, Ph.D. thesis, Imperial College London (University of London) (1985).

[41] S. Wheeler, V. Sivakumar, An elasto-plastic critical state framework for unsaturated soil, Géotechnique 45 (1) (1995) 35–53.

[42] S. S. Agus, An experimental study on hydro-mechanical characteristics of compacted bentonite-sand mixtures, Ph.D. thesis, Bauhaus-University Weimar (2005).

[43] J. Kozeny, Über kapillare leitung des wassers im boden-aufstieg, versickerung und anwendung auf die bewässerung vol, Wien: Sitzungsbericht Akademie der Wissenschaften.

[44] P. Carman, Fundamental principles of industrial filtration (a critical review of present knowledge), Trans. Inst. Chem. Eng. 16 (1938) 168–188.

[45] N.-T. Long, Coupled thermo-hydro-mechanical analysis: Experiment and back analysis, Ph.D. thesis, Ruhr-Universität Bochum (2014).

[46] R. Charlier, Approche unifiée de quelques problèmes non linéaires de mécanique des milieux continus par la méthode des éléments finis (grandes déformations des métaux et des sols, contact unilatéral de solides, conduction thermique et écoulements en milieu poreux).